

Mutual Information between Reflected and Transmitted Speckle Images

N. Fayard, A. Goetschy, R. Pierrat, and R. Carminati*

ESPCI Paris, PSL Research University, CNRS, Institut Langevin, 1 rue Jussieu, F-75005 Paris, France



(Received 10 October 2017; published 12 February 2018)

We study theoretically the mutual information between reflected and transmitted speckle patterns produced by wave scattering from disordered media. The mutual information between the two speckle images recorded on an array of N detection points (pixels) takes the form of long-range intensity correlation loops that we evaluate explicitly as a function of the disorder strength and the Thouless number g . Our analysis, supported by extensive numerical simulations, reveals a competing effect of cross-sample and surface spatial correlations. An optimal distance between pixels is proven to exist that enhances the mutual information by a factor Ng compared to the single-pixel scenario.

DOI: [10.1103/PhysRevLett.120.073901](https://doi.org/10.1103/PhysRevLett.120.073901)

When waves propagate in complex environments, their information content is spread out in space and encoded into complicated speckle patterns, eventually recorded as two-dimensional images at the output of the medium. A central issue is the quantification of the information content in speckle patterns, and its use for imaging, power deposit, or information transfer [1–3]. Much effort has been made to take advantage of the existence of spatial correlations in speckles measured in transmission. Various schemes based on the memory effect of short-range correlations (termed C_1^{TT} hereafter) have been developed to image an object through an opaque screen [4,5], while long-range correlations (C_2^{TT}), which capture nonlocal information, have been demonstrated to be useful for increasing energy delivery through turbid media [6,7].

Very recently, the existence of cross-correlations between speckle patterns measured in reflection and transmission has been demonstrated, and the shape of the intensity correlation function has been characterized in regimes ranging from quasiballistic to diffusive transport [8,9]. These correlations suggest the possibility to acquire information about a transmitted speckle from a measurement restricted to the reflection half-space. This is of crucial importance for sensing, imaging, and communicating through turbid media, and for the control of wave transmission through disordered scattering environments by wave front shaping techniques [1,2,10]. In this Letter, we quantify the amount of mutual information (MI) between transmitted and reflected speckles, and analyze the dependence of the MI on the disorder strength and the geometrical parameters characterizing the detection process (number of detectors and their interdistance). Our theory is formulated in terms of the transport mean free path (independently of the details of the microstructure), and applies for an arbitrary space dimension as long as the wave propagation remains diffusive.

The scheme of the gedanken experiment is represented in Fig. 1(a). A slab of a disordered medium is illuminated by a plane wave, and the speckle intensity profile is recorded with a CCD camera placed at the input side. The transmitted speckle, potentially recorded with another camera, is assumed to be unknown. Let $I_i^R = |E_i|^2$ be the reflected intensity measured on pixel i (or detector i) and $x_i = I_i^R / \langle I_i^R \rangle$ be the normalized intensity, the brackets $\langle \dots \rangle$ denoting an ensemble average over statistical realizations of the disordered medium. The reflected speckle image is represented by the vector \mathbf{x} of size N equal to the number of pixels of the camera. Similarly, the transmitted unknown image is wrapped up into a vector \mathbf{y} . In a statistical description of the disordered medium, configurations of disorder are generated by a stochastic process, and \mathbf{x} and \mathbf{y} are random variables. A quantitative estimate of the statistical dependence between \mathbf{x} and \mathbf{y} , or equivalently between the two speckle images, is given by their MI, defined as the difference between the entropy of \mathbf{x} and \mathbf{y} considered separately and the entropy of the pair $\{\mathbf{x}, \mathbf{y}\}$ [11]:

$$\mathcal{I} = \iint d\mathbf{x}d\mathbf{y} p(\mathbf{x}, \mathbf{y}) \log_2 \left(\frac{p(\mathbf{x}, \mathbf{y})}{p(\mathbf{x})p(\mathbf{y})} \right). \quad (1)$$

Here, $p(\mathbf{x})$, $p(\mathbf{y})$, and $p(\mathbf{x}, \mathbf{y})$ are joint probability density functions (PDFs). The MI is sensitive to all types of statistical dependence, beyond that captured by correlations. In particular, a vanishing MI is strictly equivalent to statistical independence. Moreover, it provides a direct connection with Shannon entropy and information theory concepts. Note the important difference with the study of channel capacity for multiple-input multiple-output protocols, in which the MI between input and output signals is evaluated [3,12–14]. Contrary to these protocols, here the input signal is not random, there is no external noise, and \mathbf{x} is not the injected signal but the output signal in reflection.

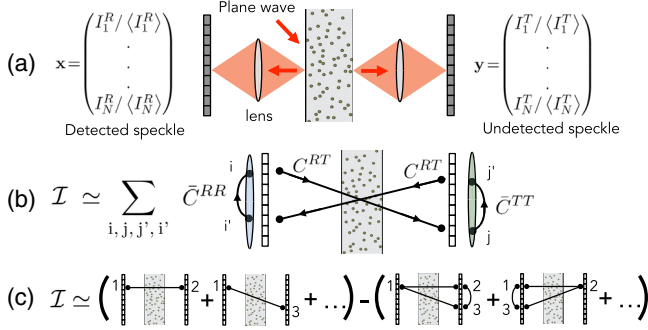


FIG. 1. (a) Schematic view of a disordered slab illuminated by a plane wave. The reflected speckle \mathbf{x} produced at the sample surface is registered on a CCD camera with N pixels, and its mutual information \mathcal{I} with the transmitted speckle \mathbf{y} is evaluated. (b) Diagrammatic representation of the trace formula (3) as a sum of correlation loops. (c) Diagrammatic representation of the approximation (6).

One difficulty in evaluating the MI lies in the fact that the PDFs $p(\mathbf{x})$, $p(\mathbf{y})$, and $p(\mathbf{x}, \mathbf{y})$ are theoretically unknown. Only marginal distributions, such as $p(x_i)$ and $p(y_i)$, as well as two-point correlations functions ($C_{ii'}^{RR} = \langle \delta x_i \delta x_{i'} \rangle$, $C_{jj'}^{TT} = \langle \delta y_j \delta y_{j'} \rangle$, and $C_{ij'}^{RT} = \langle \delta x_i \delta y_{j'} \rangle$ with $\delta x = x - 1$ and $\delta y = y - 1$) have been calculated for disordered media [9,15,16]. In the limit of small pairwise correlations, however, we will show that \mathcal{I} can be expressed as a combination of the previous correlators only, even if the field amplitudes E_i cannot be modeled as complex Gaussian random variables.

First, we express $p(\mathbf{x}, \mathbf{y})$ in terms of $p(\mathbf{x})$ and $p(\mathbf{y})$. This joint PDF is entirely characterized by the set of correlators $\langle x^{[n]} y^{[m]} \rangle = \langle x_1^{n_1} \dots x_N^{n_N} y_1^{m_1} \dots y_N^{m_N} \rangle$. Since \mathbf{x} and \mathbf{y} are weakly correlated in the multiple scattering regime [8,9], we search for leading corrections to the independent variable result $\langle x^{[n]} y^{[m]} \rangle = \langle x^{[n]} \rangle \langle y^{[m]} \rangle$. To proceed, we represent the field E_i as a sum of propagators along all possible scattering trajectories \mathcal{S} inside the medium, $E_i = \sum_{\mathcal{S}} E_i^{\mathcal{S}}$. Hence, each term $x_i^{n_i} \propto |E_i|^{2n_i}$ contains n_i replica of complex propagators $E_i^{\mathcal{S}}$ and $E_i^{\mathcal{S}*}$. The leading correction to the independent result involves all combinations of correlations between two reflection propagators and two transmission propagators. Counting these combinations yields $\langle x^{[n]} y^{[m]} \rangle = \langle x^{[n]} \rangle \langle y^{[m]} \rangle + \sum_{i,j} n_i^2 n_j^2 \langle \delta x_i \delta y_j \rangle \langle x^{[n-1_i]} \rangle \langle y^{[m-1_j]} \rangle$, where the notation $x^{[n-1_i]} = x_1^{n_1} \dots x_i^{n_i-1} \dots x_N^{n_N}$ is used. This expression gives the moments of $p(\mathbf{x}, \mathbf{y})$ in terms of the moments of $p(\mathbf{x})$ and $p(\mathbf{y})$. Then, standard algebra, detailed in the Supplemental Material [17], allows us to cast the joint PDF in the form $p(\mathbf{x}, \mathbf{y}) = p(\mathbf{x})p(\mathbf{y})[1 + \sum_{i,j} u_{ij}(\mathbf{x}, \mathbf{y})]$ with

$$u_{ij}(\mathbf{x}, \mathbf{y}) = \langle \delta x_i \delta y_j \rangle \frac{\partial_{x_i} [x_i \partial_{x_i} p(\mathbf{x})]}{p(\mathbf{x})} \frac{\partial_{y_j} [y_j \partial_{y_j} p(\mathbf{y})]}{p(\mathbf{y})}. \quad (2)$$

Second, we insert the previous decomposition into Eq. (1), and express the logarithm as a power series of

the correlation function $\sum_{ij} u_{ij}(\mathbf{x}, \mathbf{y})$. By keeping the first nonzero term in the power expansion, we obtain the following trace formula [17]:

$$\mathcal{I} \simeq \frac{1}{2 \ln 2} \text{Tr}[C^{RT} \bar{C}^{TT} C^{RT} \bar{C}^{RR}]. \quad (3)$$

In this expression we have introduced three $N \times N$ matrices, with elements defined as $C_{ij'}^{RT} = \langle \delta x_i \delta y_{j'} \rangle$,

$$\bar{C}_{jj'}^{TT} = \int d\mathbf{y} \frac{\partial_{y_j} [y_j \partial_{y_j} p(\mathbf{y})] \partial_{y_{j'}} [y_{j'} \partial_{y_{j'}} p(\mathbf{y})]}{p(\mathbf{y})}, \quad (4)$$

and $\bar{C}_{ii'}^{RR}$ in which $p(\mathbf{y})$ is replaced by $p(\mathbf{x})$. Equation (3) has a clear interpretation: the MI between the reflected and transmitted speckle patterns is the sum of all correlation loops ($i \rightarrow j \rightarrow j' \rightarrow i' \rightarrow i$), as illustrated in Fig. 1(b). In each loop, the correlation between pixels in different images is carried by pairwise cross-sample long-range coupling ($C_{ij'}^{RT}$ and $C_{j'i}^{RT}$), whereas the correlations within each image ($\bar{C}_{ii'}^{RR}$ and $\bar{C}_{jj'}^{TT}$) are more complicated since they are nonlocal, involving the full distributions $p(\mathbf{x})$ and $p(\mathbf{y})$.

To make the interpretation of the trace formula (3) even more transparent, we further assume that the distance between pixels in each image is larger than the free-space wavelength λ , so that correlations within each image remain small. As detailed in the Supplemental Material [17], this allows us to approximate the transmission PDF as $p(\mathbf{y}) = \prod_k p(y_k) [1 + \sum_{j < j'} u_{jj'}(y_j, y_{j'})]$, where $p(y_k) = e^{-y_k} [1 + C_2^{TT}(y^2/4 - y + 1/2)]$. Here, $C_2^{TT} \simeq \langle (\delta y)^2 \rangle - 1$ is the leading non-Gaussian local correction to Rayleigh statistics [25,26]. The reflection side PDF $p(\mathbf{x})$ takes the same functional form, with C_2^{RR} replacing C_2^{TT} . With this simplification, the matrix elements (4) reduce to

$$\bar{C}_{jj'}^{TT} = (1 - C_2^{TT}) \delta_{jj'} - (1 - 2C_2^{TT}) \langle \delta y_j \delta y_{j'} \rangle (1 - \delta_{jj'}). \quad (5)$$

This result is a first order expansion in C_2^{TT} that can be generalized to higher order if needed, as discussed in the Supplemental Material [17]. However, if we operate in a regime where local corrections C_2^{TT} and C_2^{RR} are much smaller than unity, we simply get $\bar{C}^{TT} = \mathbb{1} - C^{TT}$ and $\bar{C}^{RR} = \mathbb{1} - C^{RR}$, where the diagonal elements of the matrices C^{TT} and C^{RR} are zero. In this case, the trace formula (3) becomes

$$\mathcal{I} \simeq \frac{1}{2 \ln 2} \text{Tr}[(\mathbb{1} - C^{TT} - C^{RR})(C^{RT})^2]. \quad (6)$$

Hence, the existence of pairwise long-range correlations inside each image tends to reduce the MI between the two images compared to the result without surface correlation, $\text{Tr}[(C^{RT})^2]/2 \ln 2$ [see Fig. 1(c) for an illustration]. This means that long-range cross-sample correlations

and long-range surface correlations compete with each other, suggesting that a balance can be found that maximizes the MI for certain geometrical configurations of detectors. This effect is analyzed at the end of this Letter.

In order to validate the theoretical prediction (3) or its approximation (6), we have performed numerical simulations of wave propagation in two-dimensional (2D) disordered slabs with various thicknesses L and scattering mean free paths ℓ . Subwavelength dipole scatterers were placed at random positions inside the slab, and the scalar wave equation was solved numerically using the coupled-dipole method [17]. For each set of parameters, $M = 10^8$ disorder realizations were typically generated numerically, and \mathbf{x} and \mathbf{y} were calculated at the sample input and output surfaces, for various numbers N of detectors and interdistances a between detectors. Then, from the sets of data $\{\mathbf{x}_\alpha, \mathbf{y}_\alpha\}_{\alpha=1, \dots, M}$, an estimator of the MI was built, based on entropy estimates from nearest neighbor distances [17,27]. Such an estimator is expected to be more accurate than binning estimators—which consist in partitioning the support of \mathbf{x} and \mathbf{y} into bins—for which the bias potentially grows exponentially with the dimension N of \mathbf{x} and \mathbf{y} [28].

Let us first analyze the simplest situation where a single pair of detection points is considered ($N = 1$). The approximation (6) takes the simple form $\mathcal{I} \approx C^{RT}(\Delta r)^2 / 2 \ln 2$, where Δr is the transverse distance between the detection points placed on both sides of the sample. As shown in Fig. 2(a), this prediction agrees well with the direct estimate of Eq. (1), proving that the MI between \mathbf{x} and \mathbf{y} essentially boils down to the square of their correlation function C^{RT} for $N = 1$. In the multiple scattering regime ($kL \gg k\ell \gg 1$ with $k = 2\pi/\lambda$) C^{RT} is transported along diffusive paths exploring a transverse distance $\sim L$ [9], and the MI is vanishingly small for $\Delta r \gtrsim L$.

For a larger number of detectors ($N > 1$), the behavior of the MI becomes more complex. Let us analyze its

dependence on the interdistance a between detectors. Results corresponding to samples with two different thicknesses L are presented in Fig. 2(b). Here, also we obtain very good agreement between numerical estimates and the trace formula (3) completed by Eq. (5), in which the values of correlators have been obtained from simulations. This confirms that the MI in multiple scattering environments can be computed from the combination of pairwise correlators only. We distinguish three regimes in Fig. 2(b) that can be interpreted by means of the approximation (6). For detector spacing a larger than the extent L of $C^{RT}(\Delta r)$, the MI is driven by detectors placed in front of each other only. Thus, it is independent of a and N times larger than the MI obtained with a single pair of detectors with $\Delta r = 0$ [see Fig. 2(a)]. When a is progressively reduced, the MI starts to increase since more and more pairwise cross-sample correlations get activated. In the absence of correlations between the various components of \mathbf{x} or \mathbf{y} , this increase would hold for arbitrary small spacing a . However, we observe that the MI reaches a maximum for a certain critical spacing below which it falls down, thereby revealing the effect of surface correlations. The latter contain both short-range and long-range contributions [15]. Short-range contributions, responsible for the size λ of speckle spots, explain the convergence of the MI towards its $N = 1$ limit when $a \ll \lambda$. Indeed, the MI cannot be increased by adding detectors located in the same speckle spot. Nevertheless, a qualitative analysis of Eq. (6) only does not allow us to infer which contribution triggers the value of the critical distance, and to explain why the MI is globally reduced when the thickness of the medium increases.

To clarify these observations, we studied the dependence of the correlators $C^{RT}(\Delta r)$, $C^{TT}(\Delta r)$, and $C^{RR}(\Delta r)$ on L and ℓ (in the regime $kL \gg k\ell \gg 1$). Simulation results for plane wave illumination and various sets of parameters

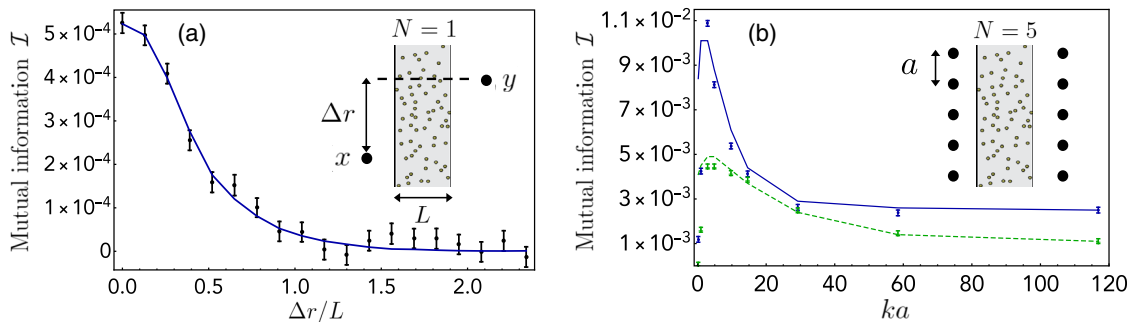


FIG. 2. MI as a function of distances between detectors. The theoretical prediction (3) (lines) is compared to the numerical estimation (dots) for various numbers of detectors N , thicknesses L , and mean free paths ℓ . (a) MI between the intensities measured in reflection ($x = I^R / \langle I^R \rangle$) and transmission ($y = I^T / \langle I^T \rangle$) versus transverse distance Δr . Parameters in the simulation: $kL = 30$, $k\ell = 10$. (b) MI between two sets of $N = 5$ detectors versus detector spacing a , for two thicknesses $kL = 30$ (solid line) and $kL = 80$ (dashed line), and fixed $k\ell = 10$. The constant residual biases in the numerical estimates (dots) have been removed, according to the procedure detailed in the Supplemental Material [17]. Note that the agreement between simulations and theory for $ka \lesssim 1$ can only be qualitative since the hypothesis of weak surface correlations is not fully satisfied.

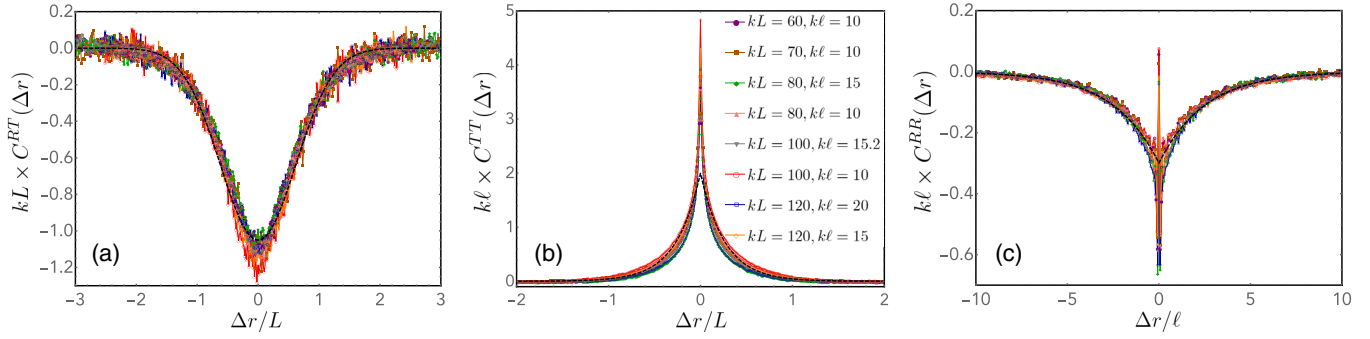


FIG. 3. Scaling of the three correlation functions that are building blocks of the MI: (a) $C^{RT}(\Delta r)$, (b) $C^{TT}(\Delta r)$, and (c) $C^{RR}(\Delta r)$. Numerical results (dots) were obtained by solving the wave equation in 2D, for different values of L and ℓ (see inset). Gaussian contributions (C_1^{TT} and C_1^{RR}), which are short range, have been removed for clarity. Dashed lines are simple fitting functions for $\Delta r \gtrsim \ell$ [Gaussian in (a) and exponentials in (b) and (c)].

$\{kL, k\ell\}$ are shown in Fig. 3. When properly normalized, data points collapse on single curves, suggesting the following scalings: $C^{RT}(\Delta r) = -f_1(\Delta r/L)/(kL)^{d-1}$ for all Δr , and $C^{TT}(\Delta r) = (L/\ell)f_2(\Delta r/L)/(kL)^{d-1}$ and $C^{RR}(\Delta r) = -f_3(\Delta r/\ell)/(k\ell)^{d-1}$ for $\Delta r \gtrsim \ell$. Here, f_1 , f_2 , and f_3 are three positive decaying functions of range and amplitude close to unity, and d is the space dimension. Theoretical justifications for these scalings are given in the Supplemental Material [17]. Note that, contrary to the well-established behavior of the long-range component of C^{TT} , C^{RT} and C^{RR} do not scale as $\sim 1/g$, where $g = k\ell(kL)^{d-2}$ is the Thouless number of a box of size L [29–31]. In particular, C^{RT} is independent of ℓ . This means that our initial assumption of weak reflection-transmission correlation is *a priori* robust against mechanisms affecting the transport mean free path, such as structural correlation of the medium [32–34], or near-field coupling between scatterers in dense materials [35–37]. We also point out that the long-range component of C^{RR} is negative, extending over a few mean free paths because waves explore such a distance in the transverse direction before being reflected [38,39]. Finally, for practical calculations, it is instructive to note that the functions f_1 , f_2 , and f_3 are reasonably well fitted by a Gaussian and two exponentials (see Fig. 3).

The simple scaling forms of the three correlators allow us to push forward the analytic calculation of the trace formula (3), in particular in the interesting limit of a large number of detectors ($N \gg 1$). As C^{RT} , C^{TT} , and C^{RR} are Toeplitz-type matrices, we may use an extension of Szegő's theorem to evaluate the trace for arbitrary spacing a [40]. To simplify the discussion, we focus on the situation where detectors (pixels) are equally spaced in all directions on the surface, in the regime $\ell \lesssim a \ll L$ (see the Supplemental Material [17] for a study in the general case). In this regime, the contribution of C^{RR} is negligible, and the remaining sums over indices in the development of the trace of the matrix product can be replaced by space integrals on the surface. The approximation (6) becomes [17]

$$\mathcal{I} \simeq \frac{N}{2 \ln 2 [(kL)(ka)]^{d-1}} \left(c_{RT} - \frac{c_{TT}}{(ka)^{d-1}} \frac{L}{\ell} \right), \quad (7)$$

where $c_{RT} = \int d\mathbf{r} f_1(r)^2$ and $c_{TT} = \iint d\mathbf{r} d\mathbf{r}' f_1(r) f_2(r') \times f_1(|\mathbf{r} + \mathbf{r}'|)$ are two numerical constants of order unity. The result in Eq. (7) supports previous qualitative observations: the MI scales linearly with the number of detectors, and decreases when the sample thickness increases because the cross-sample correlation C^{RT} itself is reduced. Interestingly, when we normalize Eq. (7) by the MI measured for a single detector $\mathcal{I}_1 = C^{RT}(0)^2/2 \ln 2$, we obtain $\mathcal{I}/\mathcal{I}_1 \propto N(c_{RT}u - c_{TT}u^2/g)$, where $u = (L/a)^{d-1}$. This shows that \mathcal{I} exhibits a maximum triggered by the long-range component of C^{TT} , of the form $\mathcal{I}^{\max} \sim Ng\mathcal{I}_1$, for a critical interdistance a^* much larger than the wavelength and potentially larger than ℓ [$(L/a^*)^{d-1} = (c_{RT}/2c_{TT})g$ so that $a^* \sim \lambda(L/\ell)^{1/(d-1)}$]. Hence, the MI for an array of N detectors with optimized interdistance is enhanced by a factor $Ng \gg 1$ compared to the MI for a single detector. These considerations are confirmed in Fig. 4 by the good agreement between the numerical

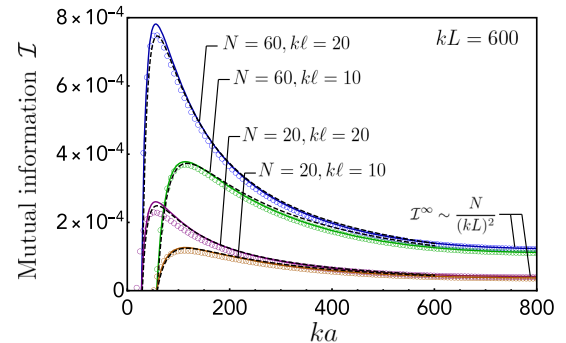


FIG. 4. MI computed from the trace formula (6). Open circles are numerical calculations of the trace, using the scaling functions for C^{RT} , C^{TT} , and C^{RR} identified in Fig. 3. Solid lines stand for the analytic result presented in the Supplemental Material [17], and dashed lines for its approximation (7) valid for $\ell \lesssim a \lesssim L$.

evaluation of the trace (6) and the full analytic prediction detailed in the Supplemental Material [17] and its approximation (7). In particular, denoting by $\mathcal{I}^\infty = N\mathcal{I}_1$ the MI obtained in the large spacing regime $a \gtrsim L$ where only front side correlations contribute, we clearly observe the enhancement factor $\mathcal{I}^{\max}/\mathcal{I}^\infty \sim g$.

In summary, we have presented a quantitative treatment of the MI between two speckle images produced on opposite sides of a multiple scattering medium. The dependence of the MI on length scales characterizing the medium and on the detection geometry highlights the entangled and competitive contributions of long-range intensity correlations. In particular, using an array of N detectors with interdistance a to record the speckle image, the MI can be increased by a factor of Ng compared to the single detector case for a critical value of $a \gg \lambda$. This enhancement factor could guide the development of experimental protocols to measure the MI, in configurations such as that in Ref. [9] for which Ng can be made very large. Although our approach does not give the recipe to recover from \mathbf{x} the information contained in \mathbf{y} , or vice versa, it provides quantitative estimates of the MI, and conditions for its optimization, that should help the design of new setups dedicated to information recovery or transfer in complex media.

This research was supported by LABEX WIFI (Laboratory of Excellence within the French Program Investments for the Future) under references ANR-10-LABX-24 and ANR-10-IDEX-0001-02 PSL*. N. F. acknowledges financial support from the French Direction Générale de l'Armement (DGA).

*remi.carminati@espci.fr

- [1] A. P. Mosk, A. Lagendijk, G. Lerosey, and M. Fink, *Nat. Photonics* **6**, 283 (2012).
- [2] S. Rotter and S. Gigan, *Rev. Mod. Phys.* **89**, 015005 (2017).
- [3] A. Moustakas, H. Baranger, L. Balents, A. Sengupta, and S. Simon, *Science* **287**, 287 (2000).
- [4] J. Bertolotti, E. G. van Putten, C. Blum, A. Lagendijk, W. L. Vos, and A. P. Mosk, *Nature (London)* **491**, 232 (2012).
- [5] O. Katz, P. Heidmann, M. Fink, and S. Gigan, *Nat. Photonics* **8**, 784 (2014).
- [6] S. M. Popoff, A. Goetschy, S. F. Liew, A. D. Stone, and H. Cao, *Phys. Rev. Lett.* **112**, 133903 (2014).
- [7] C. W. Hsu, S. F. Liew, A. Goetschy, H. Cao, and A. D. Stone, *Nat. Phys.* **13**, 497 (2017).
- [8] N. Fayard, A. Cazé, R. Pierrat, and R. Carminati, *Phys. Rev. A* **92**, 033827 (2015).
- [9] I. Starshynov, A. M. Paniagua-Diaz, N. Fayard, A. Goetschy, R. Pierrat, R. Carminati, and J. Bertolotti, [arXiv:1707.03622](https://arxiv.org/abs/1707.03622).
- [10] S. H. Simon, A. L. Moustakas, M. Stoychev, and H. Safar, *Phys. Today* **54**, No. 9 38 (2001).
- [11] T. M. Cover and J. A. Thomas, *Elements of Information Theory* (Wiley, New York, 1991).
- [12] A. M. Tulino and S. Verdú, *Random Matrix Theory and Wireless Communications* (Now Publishers, Delft, 2004).
- [13] S. E. Skipetrov, *Phys. Rev. E* **67**, 036621 (2003).
- [14] A. Goetschy and A. D. Stone, *Phys. Rev. Lett.* **111**, 063901 (2013).
- [15] E. Akkermans and G. Montambaux, *Mesoscopic Physics of Electrons and Photons* (Cambridge University Press, Cambridge, England, 2007).
- [16] M. C. W. van Rossum and T. M. Nieuwenhuizen, *Rev. Mod. Phys.* **71**, 313 (1999).
- [17] See Supplemental Material at <http://link.aps.org/supplemental/10.1103/PhysRevLett.120.073901>, which includes Refs. [18–24], that contains (1) the proof of the trace formula; (2) details about wave propagation simulation; (3) an analysis of the mutual information estimator and its bias for various N ; (4) a justification of the scaling form of long-range correlation functions; (5) the analytic calculation of the trace formula based on properties of Toeplitz matrices.
- [18] E. Kogan and M. Kaveh, *Phys. Rev. B* **52**, R3813 (1995).
- [19] T. M. Nieuwenhuizen and M. C. W. van Rossum, *Phys. Rev. Lett.* **74**, 2674 (1995).
- [20] M. Lax, *Phys. Rev.* **85**, 621 (1952).
- [21] C. W. J. Beenakker, *Rev. Mod. Phys.* **69**, 731 (1997).
- [22] D. B. Rogozkin and M. Y. Cherkasov, *Phys. Lett. A* **214**, 292 (1996).
- [23] P. A. Mello, *J. Phys. A* **23**, 4061 (1990).
- [24] P. A. Mello, E. Akkermans, and B. Shapiro, *Phys. Rev. Lett.* **61**, 459 (1988).
- [25] N. Shnerb and M. Kaveh, *Phys. Rev. B* **43**, 1279 (1991).
- [26] E. Kogan, M. Kaveh, R. Baumgartner, and R. Berkovits, *Phys. Rev. B* **48**, 9404 (1993).
- [27] A. Kraskov, H. Stögbauer, and P. Grassberger, *Phys. Rev. E* **69**, 066138 (2004).
- [28] R. Moddemeijer, *Signal Processing* **16**, 233 (1989).
- [29] M. J. Stephen and G. Cwilich, *Phys. Rev. Lett.* **59**, 285 (1987).
- [30] S. Feng, C. Kane, P. A. Lee, and A. D. Stone, *Phys. Rev. Lett.* **61**, 834 (1988).
- [31] R. Pnini and B. Shapiro, *Phys. Rev. B* **39**, 6986 (1989).
- [32] S. Fraden and G. Maret, *Phys. Rev. Lett.* **65**, 512 (1990).
- [33] L. F. Rojas-Ochoa, J. M. Mendez-Alcaraz, J. J. Sáenz, P. Schurtenberger, and F. Scheffold, *Phys. Rev. Lett.* **93**, 073903 (2004).
- [34] O. Leseur, R. Pierrat, and R. Carminati, *Optica* **3**, 763 (2016).
- [35] T. Nieuwenhuizen, A. Burin, Y. Kagan, and G. Shlyapnikov, *Phys. Lett. A* **184**, 360 (1994).
- [36] A. Dogariu and R. Carminati, *Phys. Rep.* **559**, 1 (2015).
- [37] R. Rezvani Naraghi, S. Sukhov, J. J. Sáenz, and A. Dogariu, *Phys. Rev. Lett.* **115**, 203903 (2015).
- [38] D. B. Rogozkin and M. Y. Cherkasov, *Phys. Rev. B* **51**, 12256 (1995).
- [39] L. Froufe-Pérez, A. Garcia-Martin, G. Cwilich, and J. Saenz, *Physica (Amsterdam)* **386A**, 625 (2007).
- [40] R. M. Gray, *Found. Trends Commun. Inf. Theory* **2**, 155 (2006).